Structures of complexes formed by organophosphorus acid extractants and divalent metal ions

Stijn Raiguel[†*], Femke Derison[†], Koen Binnemans[†]

[†] KU Leuven, Department of Chemistry, Celestijnenlaan 200F, P.O. box 2404, B-3001 Leuven, Belgium.

*Corresponding author:
Email: Stijn.Raiguel@kuleuven.be

Supplementary Information

Table of contents

Slope analysis of extraction equilibria

The general form of an extraction by an acidic extractant can be written as:

$$j\,M^{n+} + j\,(\frac{n}{2} + m)\,(\bar{HA})_2 \rightleftharpoons [MA_n(\bar{HA}_2)_m]_j + j\,n\,H^+ \qquad \text{(Eq. S1)}$$

where overbars denote organic phase species, M represents the extracted metal and HA is the extractant, which occurs as a dimer in the organic phase. The associated equilibrium constant K_{eq} takes the form:

$$K_{eq} = \frac{\left[\left[MA_n(HA_2)_m\right]_j\right]\,[H^+]^{j\,n}}{[M^{n+}]^j\,[(HA)_2]^{j\,(\frac{n}{2}+m)}} \qquad \text{(Eq. S2)}$$

Taking the base 10 logarithm and rearranging yields:

$$\mathrm{j}\log[M^{n+}]_{aq} - \log\frac{[M]_{org}}{j} = j\,n\log[H^+] - j\left(\frac{n}{2}+m\right)\log[(HA)_2] - \log K_{eq} \qquad \text{(Eq. S3)}$$

With subscripts *aq* and *org* denoting analytical aqueous and organic concentrations, respectively. Note that in the main text, the value of (n/2 + m) is defined as q. Substituting the definition of pH and distribution ratio D yields:

$$\log j\,D = j\,n\,pH + (j-1)\log[M]_{aq} + j\left(\frac{n}{2}+m\right)\log[(HA)_2] + \log K_{eq} \qquad \text{(Eq. S4)}$$

At lower loading (< 50%), when the extracted complex is generally monomeric (j = 1), this simplifies to:

$$\log D = n\,pH + \left(\frac{n}{2}+m\right)\log[(HA)_2] + \log K_{eq} \qquad \text{(Eq. S5)}$$

This expression allows the determination of coefficients in extraction equilibria by linear regression analysis of log$D$ versus the logarithm of a variable concentration of the reactant of interest. Other concentrations should be constant or at least determined with reasonable accuracy and mathematically taken into account. This method is only effective provided that a number of assumptions are met, including immiscibility of the phases, absence of ionic strength effects and invariability speciation and extraction mechanism within the studied range.

This method also requires knowledge of the equilibrium concentration of the extractant, [(HA)$_2$], which may differ significantly from the initial concentration. At low loading, the equilibrium concentration can be estimated from the initial concentration by subtracting the assumed number of dimers involved in the complexation of the metal ion. This number, in turn, is estimated by determining the organic phase concentration of the metal and assuming a value for m (Eq. S1). If the experimental slope of log$D$ as a function of log[(HA)$_2$] is in agreement with the hypothetical value for m, the hypothesis can be considered reasonably founded.

As an illustrative example, Co(II), extracted as Co(HA_2)$_2$ at low loading. Two extractant dimers are thus involved in complexation with Co(II), and hence the analysis is expected to yield a value of m = 1 (with n = 2). The experiment is carried out by varying the initial concentration of the extractant in the organic phase, while keeping other parameters constant. At equilibrium, the distribution of Co(II) and the pH are determined experimentally. For each data point, 2 extractant dimers are subtracted from the initial extractant concentration per Co(II) ion in the organic phase, *i.e.* $[(HA)_2]_{eq} = [(HA)_2]_{initial} - 2[Co]_{org}$. As the pH will be variable in this experimental setup, Eq. S5 is rearranged to plot log$D$ – 2 pH as a function of log$[(HA)_2]$, yielding a linear curve with slope (n/2 + m) = 2. If the hypothetical value of m = 1 does not yield a slope of 1, the hypothesis is rejected.

Additional FT-IR data

Cobalt(II)

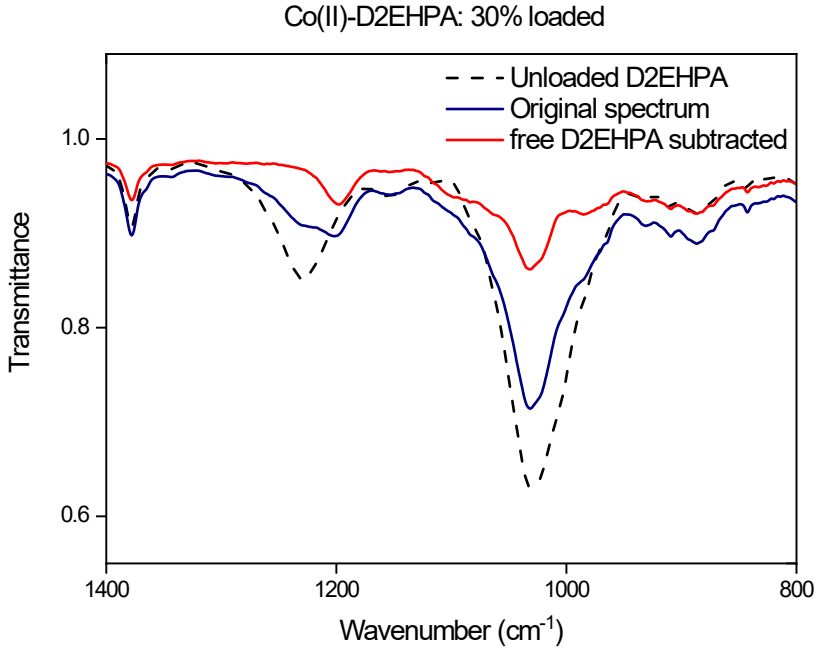

Fig. S1: FT-IR spectrum of D2EHPA (245 g L^{-1} in heptane) before and after loading with cobalt(II) to a loading of 30%. The red spectrum shows the spectrum of loaded D2EHPA after subtraction of the spectrum of unloaded D2EHPA, scaled by 40%, to remove background caused by absorption by free (unloaded) D2EHPA.

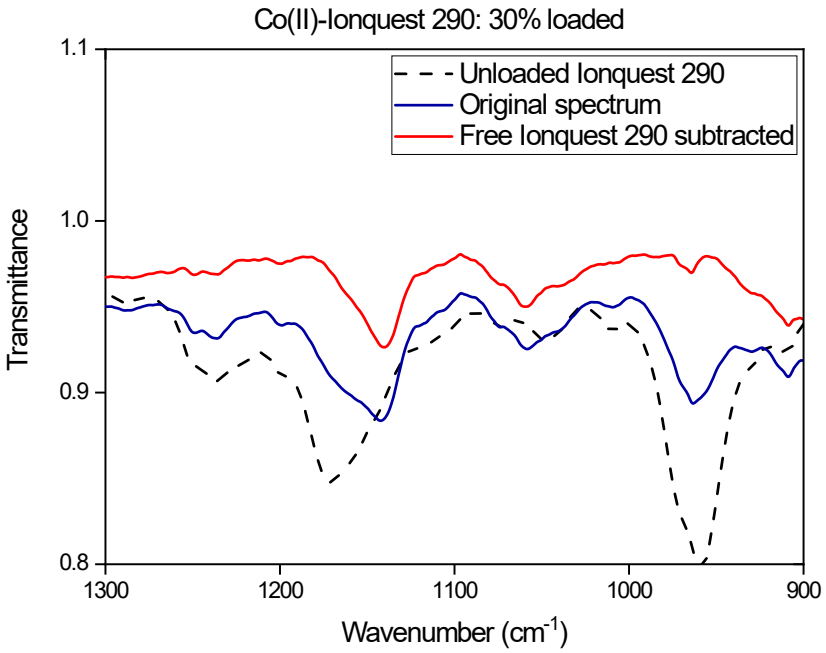

Fig. S2: FT-IR spectrum of Ionquest 290 (183 g L^{-1} in heptane) before and after loading with cobalt(II) to a loading of 30%. The red spectrum shows the spectrum of loaded D2EHPA after subtraction of the spectrum of unloaded Ionquest 290, scaled by 40%, to remove background caused by absorption by free (unloaded) D2EHPA.

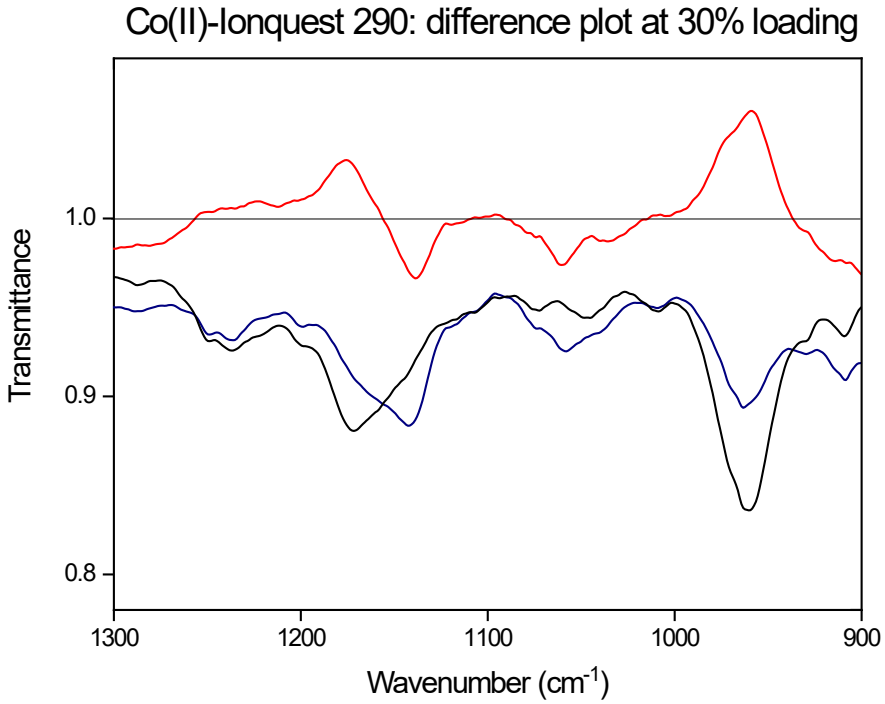

Fig. S3: FT-IR spectrum of Ionquest 290 (183 g L^{-1} in heptane) before and after loading with cobalt(II) to a loading of 50%. The red spectrum shows the difference of the two spectra, removing background signals and revealing the location of nascent and evanescent signals.

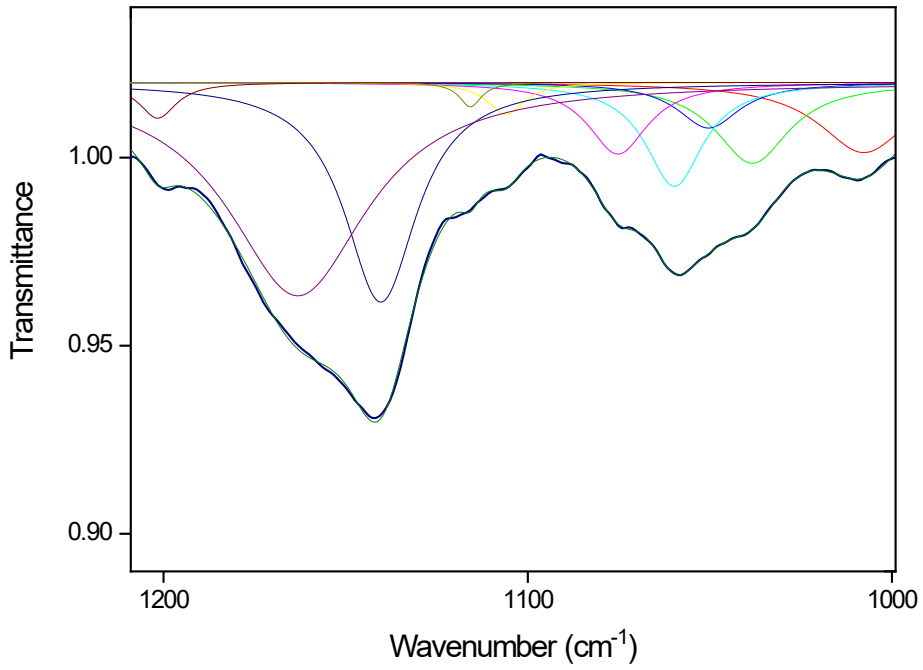

Fig. S4: Deconvolution of the FT-IR spectrum of Ionquest 290 (183 g L^{-1} in heptane) after loading with cobalt(II) to a loading of 50%. A linear baseline was subtracted prior to application of a 10-peak Lorentzian regression. The red, royal blue and magenta peaks correspond to the background signals observed in unloaded Ionquest 290, while the green and cyan peaks correspond to bound phosphinate absorption bands (Fig. S3).

Table S1: peak locations in FT-IR spectra for the Co(II)-D2EHPA and cobalt(II)–Ionquest 290 systems. Shoulders are denoted by (s).

Condition	PO_2 antisymmetrical stretching	PO_2 symmetrical stretching
D2EHPA, 30% loaded[a]	1198	1032
D2EHPA, 50% loaded	1198	1032
D2EHPA, 100% loaded	1184	1104, 1064, 1055, 1035
Ionquest 290, 30% loaded, deconvolution[b]	1140	1059, 1038
Ionquest 290, 50% loaded	1138	1059, 1040(s)
Ionquest 290, 100% loaded	1128	1056, 1040

[a]*After subtraction of the spectrum of unloaded D2EHPA, scaled by 40%, to remove background caused by absorption by free (unloaded) D2EHPA.*
[b]*A linear baseline was subtracted prior to application of a 10-peak Lorentzian regression. Maxima of fitted peaks are given.*

Nickel(II)

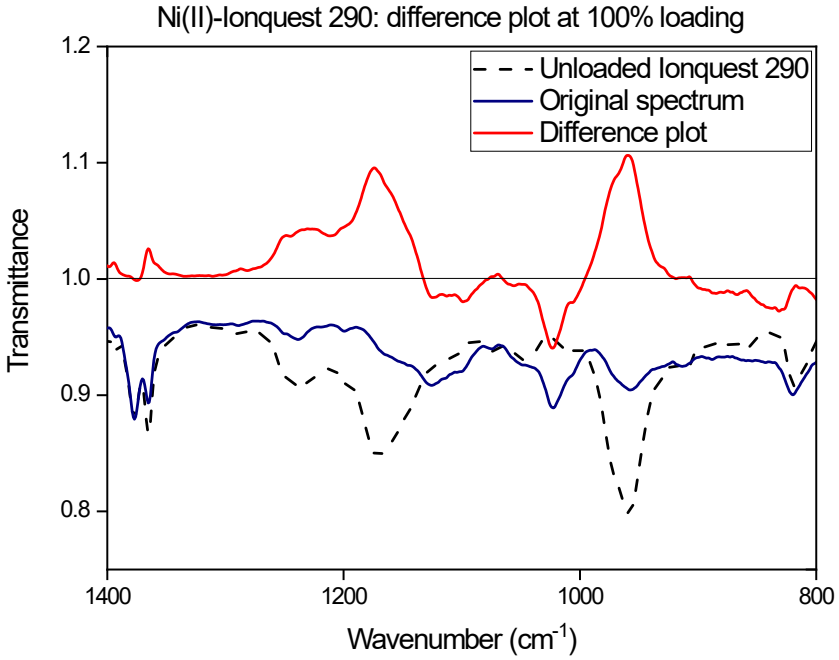

Fig. S5: FT-IR spectrum of Ni(II)–Ionquest 290 (30 vol% Ionquest 290 in Exxsol D120) before and after loading. The red spectrum shows the difference of the two spectra, removing background signals and revealing the location of nascent and evanescent signals.

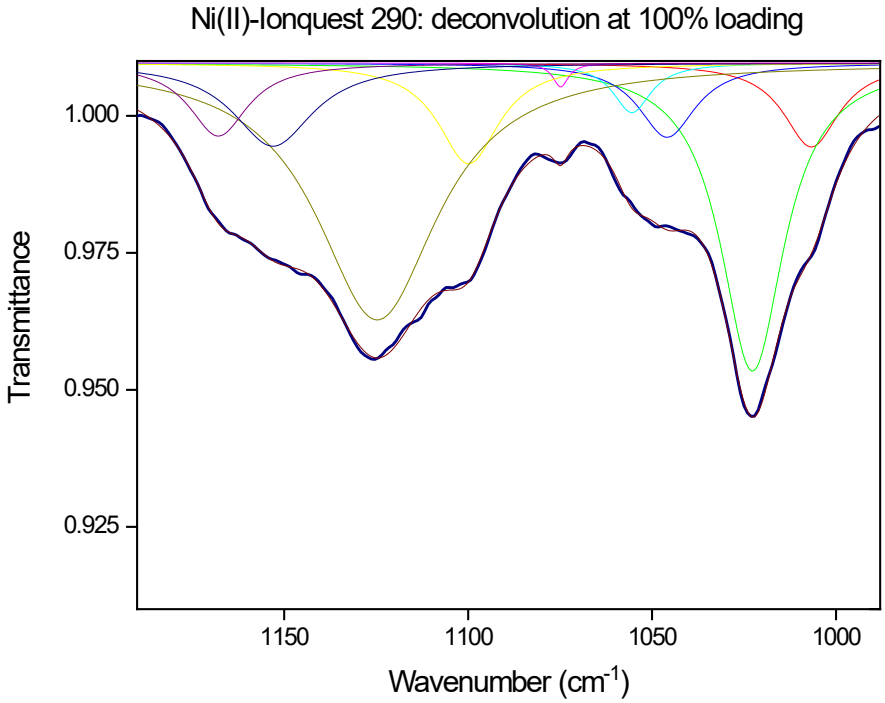

Fig. S6: Deconvolution of the FT-IR spectrum of Ni(II)–Ionquest 290 (30 vol% Ionquest 290 in Exxsol D120) at a loading of 100%. A linear baseline was subtracted prior to application of a 9-peak Lorentzian regression. The red, royal blue and magenta peaks correspond to the background signals observed in unloaded Ionquest 290, while the green and cyan peaks correspond to phosphinate absorption bands (Fig. S5).

Table S2: peak locations in FT-IR spectra for the Ni(II)-D2EHPA and Ni(II)–Ionquest 290 systems. Shoulders are denoted by (s).

Condition	PO_2 antisymmetrical stretching	PO_2 symmetrical stretching
D2EHPA, 100% loaded	1192	1083, 1065, 1054(s), 1032, 1021
Ionquest 290, 100% loaded, deconvolution[a]	1125, 1100	1055, 1023

[a]*A linear baseline was subtracted prior to application of a 9-peak Lorentzian regression. Maxima of fitted peaks are given.*

Magnesium(II)

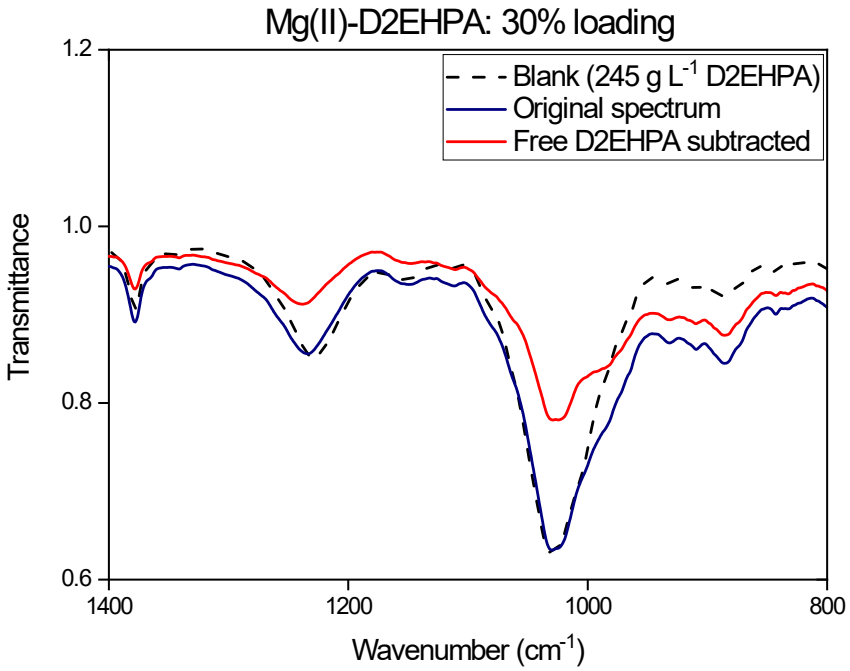

Fig. S7: FT-IR spectrum of D2EHPA (245 g L^{-1} in heptane) before and after loading with magnesium(II) to a loading of 30%. The red spectrum shows the spectrum of loaded D2EHPA after subtraction of the spectrum of unloaded D2EHPA, scaled by 40%, to remove background caused by absorption by free (unloaded) D2EHPA.

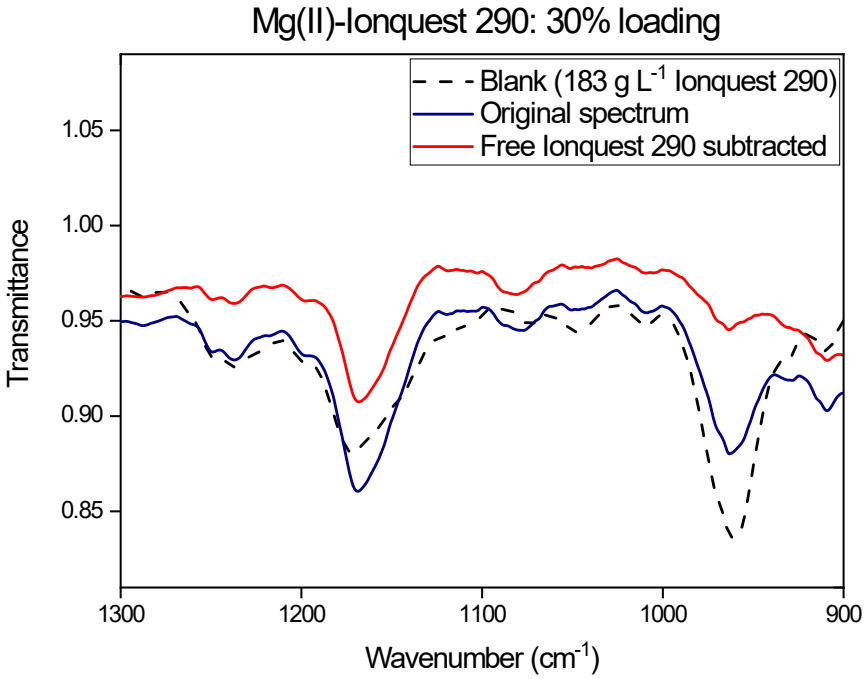

Fig. S8: FT-IR spectrum of Ionquest 290 (183 g L^{-1} in heptane) before and after loading with magnesium(II) to a loading of 30%. The red spectrum shows the spectrum of loaded Ionquest 290 after subtraction of the spectrum of unloaded Ionquest 290, scaled by 40%, to remove background caused by absorption by free (unloaded) Ionquest 290.

Table S3: peak locations in FT-IR spectra for the Mg(II)–D2EHPA and Mg(II)–Ionquest 290 systems.

Condition	PO_2 antisymmetrical stretching	PO_2 symmetrical stretching
D2EHPA, 30% loaded[a]	1238	1029
D2EHPA, 50% loaded	1234	1032
D2EHPA, 100% loaded	1216	1134, 1114, 1066, 1037
Ionquest 290, 50% loaded[a]	1168	n.d.[b]
Ionquest 290, 50% loaded	1168	n.d.[b]
Ionquest 290, 100% loaded	1165	1086

[a]*After subtraction of the spectrum of unloaded D2EHPA, scaled by 40%, to remove background caused by absorption by free (unloaded) D2EHPA.*
[b]*None detected.*

Calcium(II)

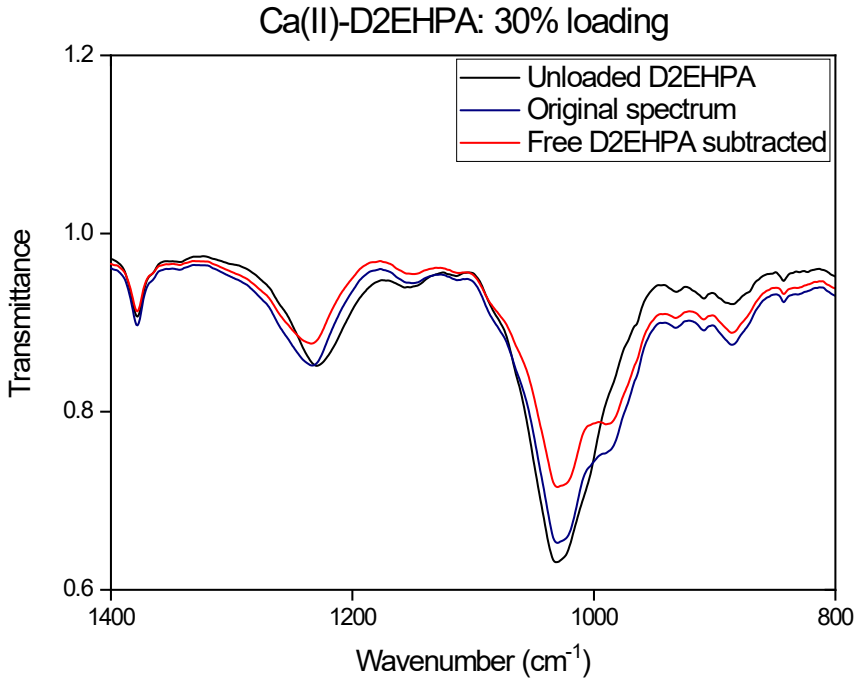

Fig. S9: FT-IR spectrum of D2EHPA (241 g L^{-1} in heptane) before and after loading with calcium(II) to a loading of 33%. The red spectrum shows the spectrum of loaded D2EHPA after subtraction of the spectrum of unloaded D2EHPA, scaled by 34%, to remove background caused by absorption by free (unloaded) D2EHPA.

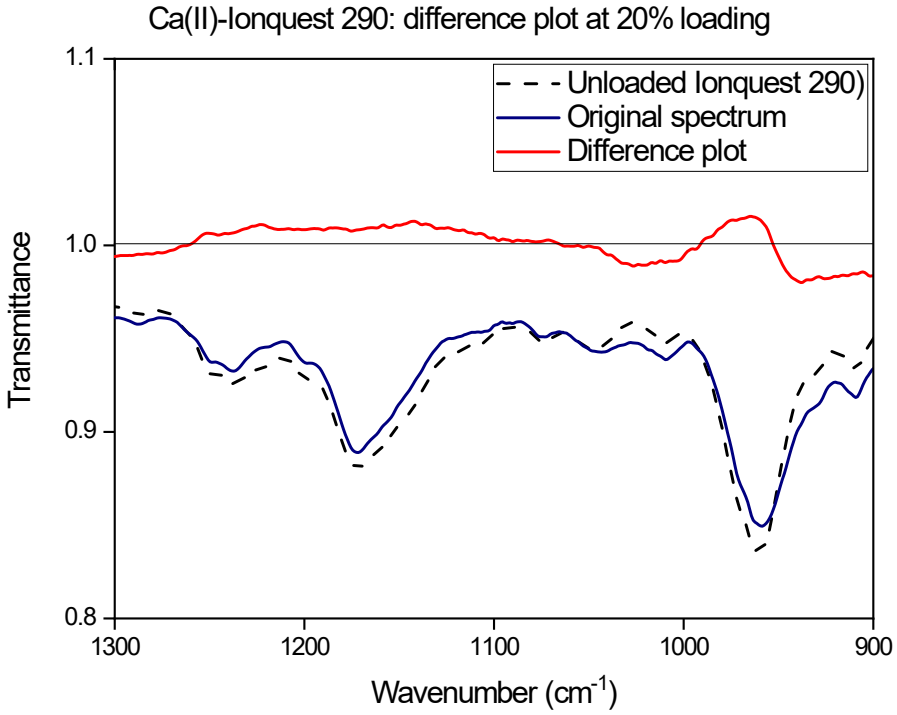

Fig. S10: FT-IR spectrum of Ionquest 290 (183 g L^{-1} in heptane) before and after loading with calcium(II) to a loading of 40%. The red spectrum shows the difference of the two spectra, removing background signals and revealing the location of nascent and evanescent signals.

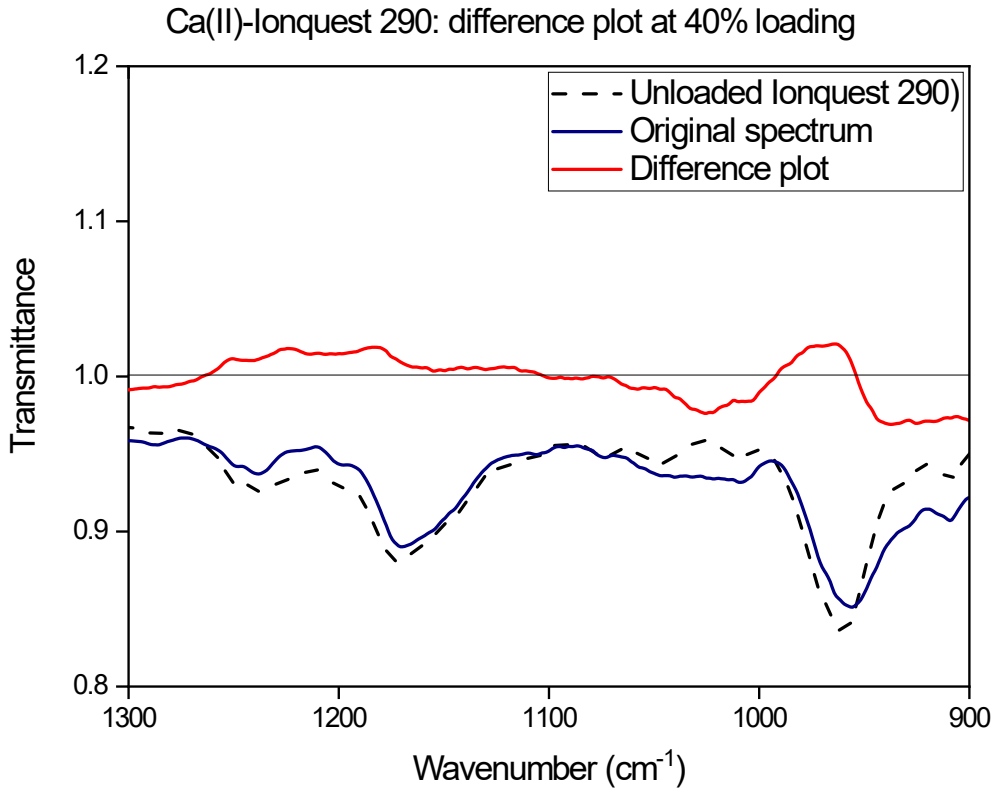

Fig. S11: FT-IR spectrum of Ionquest 290 (183 g L^{-1} in heptane) before and after loading with calcium(II) to a loading of 20%. The red spectrum shows the difference of the two spectra, removing background signals and revealing the location of nascent and evanescent signals.

Table S4: peak locations in FT-IR spectra for the Ca(II)–D2EHPA and Ca(II)–Ionquest 290 systems. Shoulders are denoted by (s).

Condition	PO_2 antisymmetrical stretching	PO_2 symmetrical stretching
D2EHPA, 30% loaded[a]	1234	1030, 990
D2EHPA, 50% loaded	1225	1032
D2EHPA, 100% loaded	1209	1099, 1086(s), 1063, 1054, 1033
Ionquest 290, 20% loaded	1172	1026[b]
Ionquest 290, 40% loaded	1170	1058[b], 1026[b]

[a]*After subtraction of the spectrum of unloaded D2EHPA, scaled by 34%, to remove background caused by absorption by free (unloaded) D2EHPA.*
[b]*After subtraction of the spectrum of unloaded Ionquest 290.*

Manganese(II)

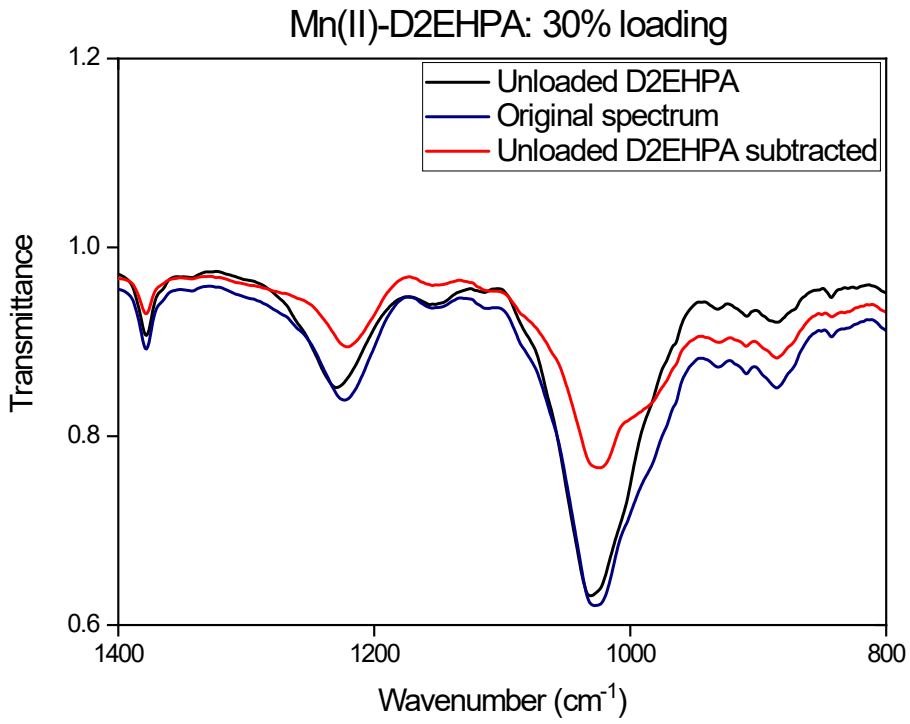

Fig. S12: FT-IR spectrum of D2EHPA (245 g L^{-1} in heptane) before and after loading with manganese(II) to a loading of 30%. The red spectrum shows the spectrum of loaded D2EHPA after subtraction of the spectrum of unloaded D2EHPA, scaled by 40%, to remove background caused by absorption by free (unloaded) D2EHPA.

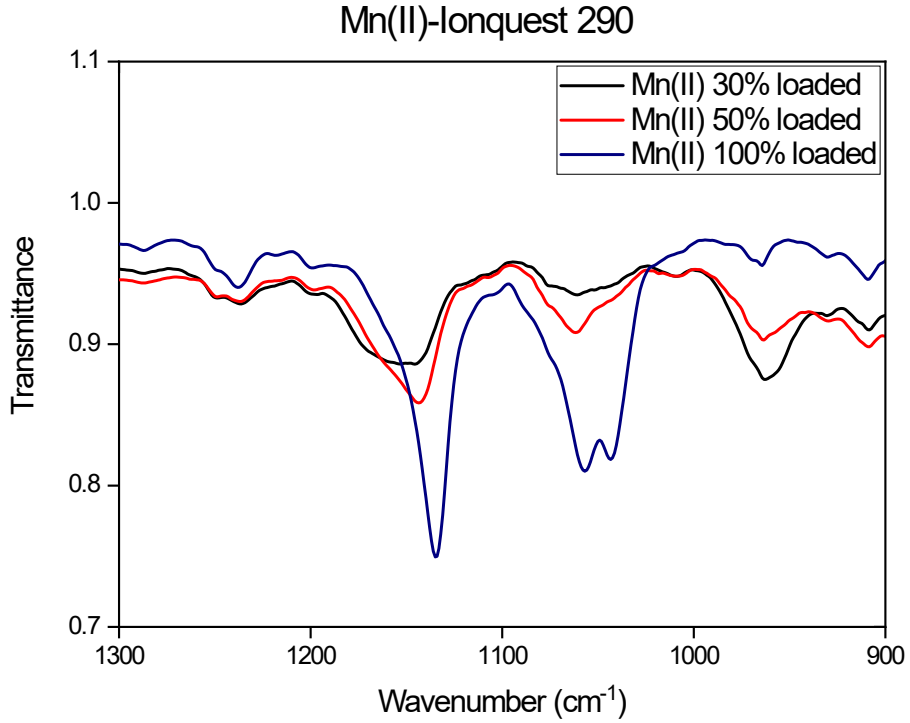

Fig. S13: FT-IR spectra of Ionquest 290 (183 g L^{-1} in heptane) after loading with manganese(II).

Table S5: peak locations in FT-IR spectra for the Mn(II)-D2EHPA and Mn(II)-Ionquest 290 systems. Shoulders are denoted by (s).

Condition	PO_2 antisymmetrical stretching	PO_2 symmetrical stretching
D2EHPA, 30% loaded[a]	1221	1023
D2EHPA, 50% loaded	1213	1031
D2EHPA, 100% loaded	1195	1105, 1064, 1055, 1035
Ionquest 290, 30% loaded[b]	1146	1062, 1045(s)
Ionquest 290, 50% loaded	1144	1062, 1046(s)
Ionquest 290, 100% loaded	1135	1057, 1043

[a]*After subtraction of the spectrum of unloaded D2EHPA, scaled by 40%, to remove background caused by absorption by free (unloaded) D2EHPA.*
[b]*Unloaded Ionquest 290 not subtracted.*

Copper(II)

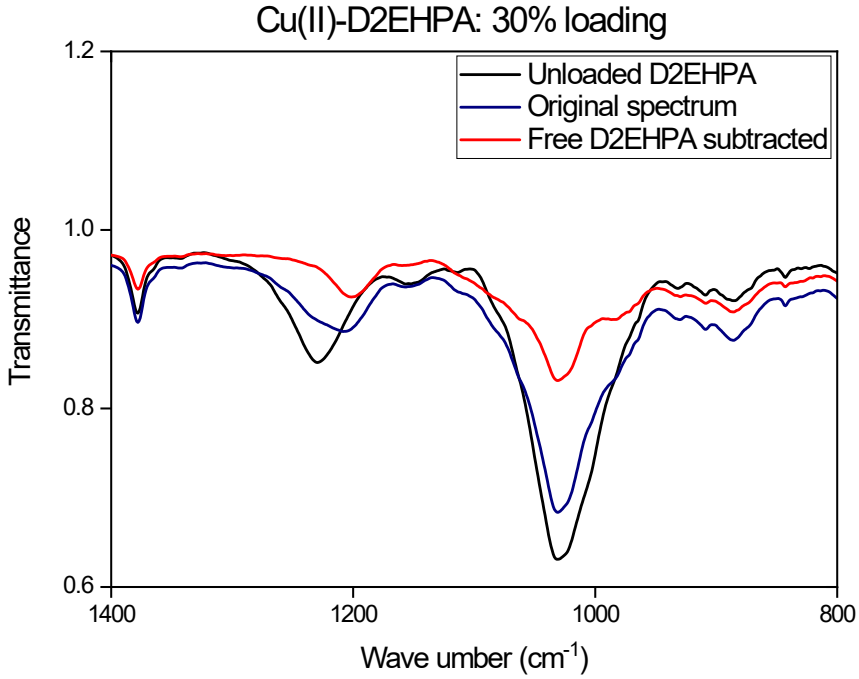

Fig. S14: FT-IR spectrum of D2EHPA (245 g L^{-1} in heptane) before and after loading with copper(II) to a loading of 30%. The red spectrum shows the spectrum of loaded D2EHPA after subtraction of the spectrum of unloaded D2EHPA, scaled by 40%, to remove background caused by absorption by free (unloaded) D2EHPA.

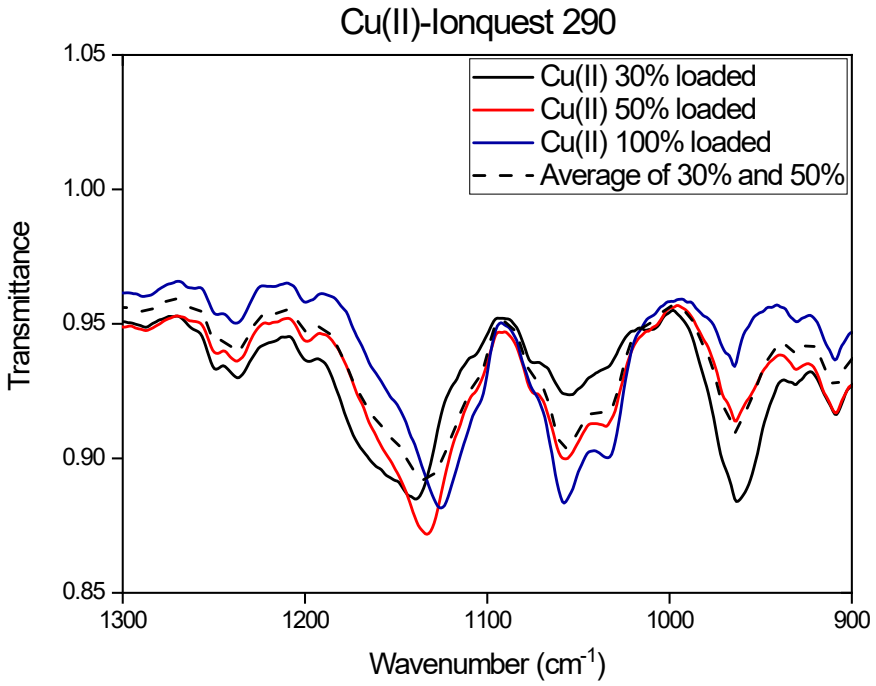

Fig. S15: FT-IR spectra of Ionquest 290 (183 g L^{-1} in heptane) after loading with copper(II). For comparison, the normalized sum (average) of the spectra at 30% and 50% loading is also given, demonstrating that the maxima of the spectrum at 50% loading are reproduced by superposition of the spectra of these species.

Table S6: peak locations in FT-IR spectra for the Cu(II)-D2EHPA and Cu(II)-Ionquest 290 systems. Shoulders are denoted by (s).

Condition	PO_2 antisymmetrical stretching	PO_2 symmetrical stretching
D2EHPA, 30% loaded[a]	1202	1031
D2EHPA, 50% loaded	1197	1031
D2EHPA, 100% loaded	1222, 1182	1099, 1082, 1063, 1053, 1035
Ionquest 290, 30% loaded[b]	1140	1055, 1035(s)
Ionquest 290, 50% loaded	1133	1057, 1035(s)
Ionquest 290, 100% loaded	1125	1058, 1035(s)

[a]*After subtraction of the spectrum of unloaded D2EHPA, scaled by 40%, to remove background caused by absorption by free (unloaded) D2EHPA.*

[b]*Unloaded Ionquest 290 not subtracted.*

Zinc(II)

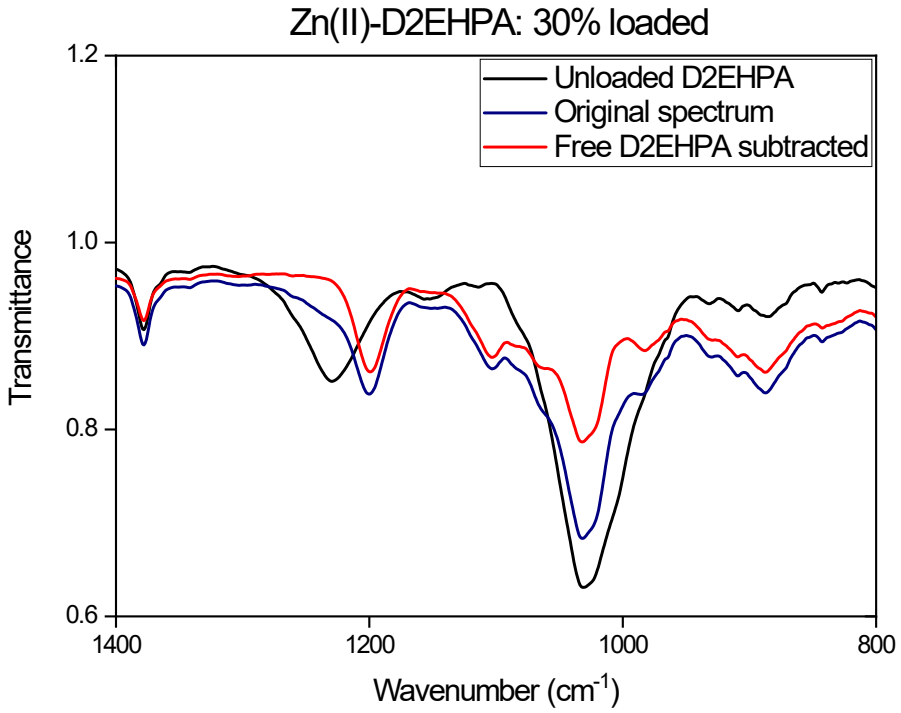

Fig. S16: FT-IR spectrum of D2EHPA (245 g L^{-1} in heptane) before and after loading with zinc(II) to a loading of 30%. The red spectrum shows the spectrum of loaded D2EHPA after subtraction of the spectrum of unloaded D2EHPA, scaled by 28%, to remove background caused by absorption by free (unloaded) D2EHPA.

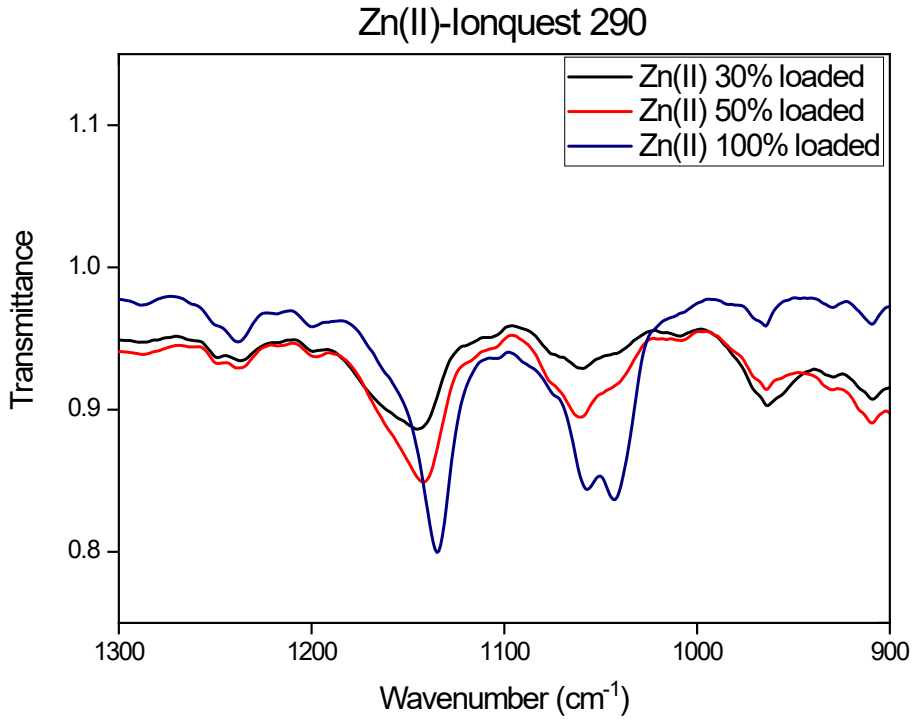

Fig. S17: FT-IR spectra of Ionquest 290 (183 g L^{-1} in heptane) after loading with zinc(II).

Table S7: peak locations in FT-IR spectra for the Zn(II)-D2EHPA and Zn(II)-Ionquest 290 systems. Shoulders are denoted by (s).

Condition	PO_2 antisymmetrical stretching	PO_2 symmetrical stretching
D2EHPA, 30% loaded[a]	1200	1103, 1032
D2EHPA, 50% loaded	1199	1104, 1032
D2EHPA, 100% loaded	1189	1099, 1066, 1057(s), 1034
Ionquest 290, 30% loaded[b]	1146	1059, 1041(s)
Ionquest 290, 50% loaded	1142	1061, 1042(s)
Ionquest 290, 100% loaded	1135	1057, 1043

[a]*After subtraction of the spectrum of unloaded D2EHPA, scaled by 28%, to remove background caused by absorption by free (unloaded) D2EHPA.*

[b]*Unloaded Ionquest 290 not subtracted.*

DSC traces

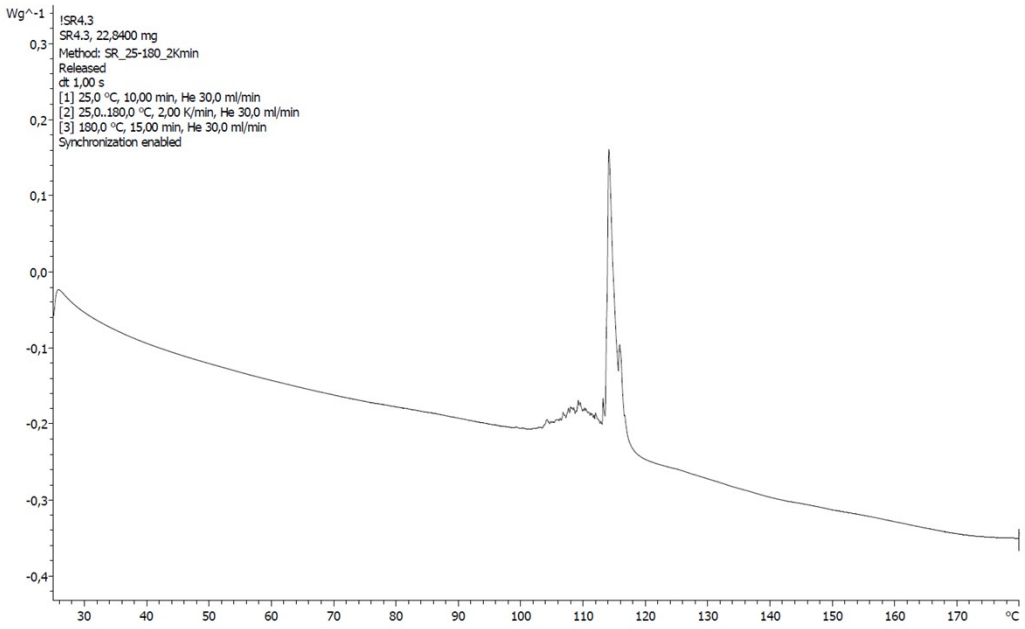

Fig. S18: DSC trace of D2EHPA (30 wt% in Exxsol D120), 100% loaded with Ni(II) up to 180 °C. Heat flow is defined such that a positive flow corresponds to an endothermic event.

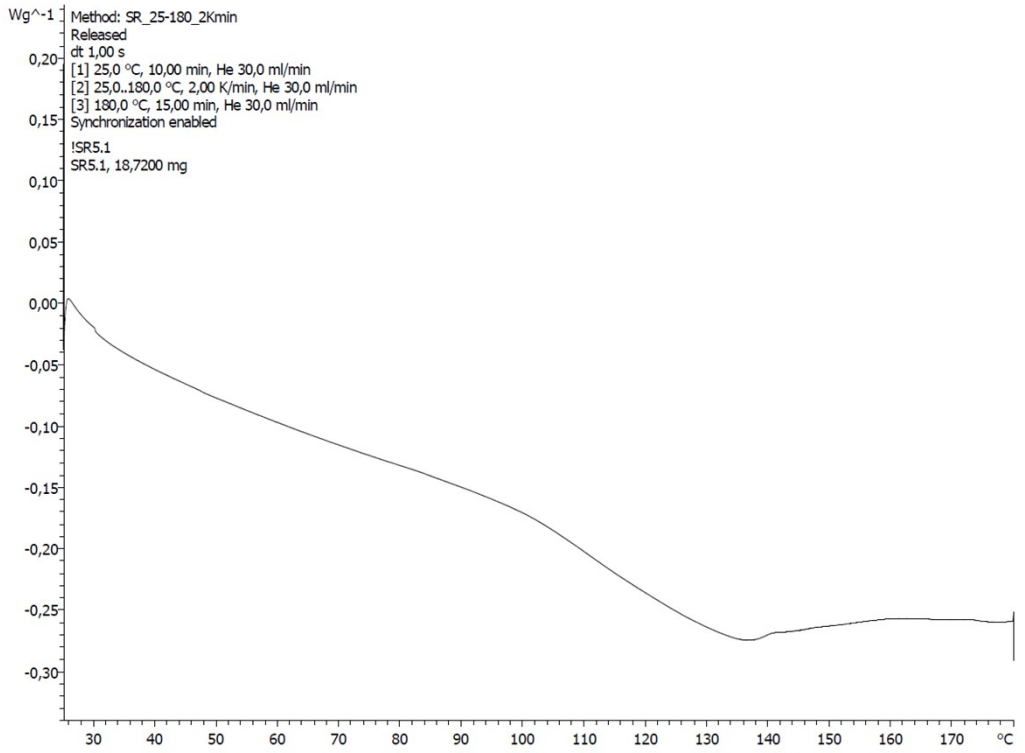

Fig. S19: DSC trace of Ionquest 290 (30 wt% in Exxsol D120), 100% loaded with Ni(II) up to 180 °C. Heat flow is defined such that a positive flow corresponds to an endothermic event.

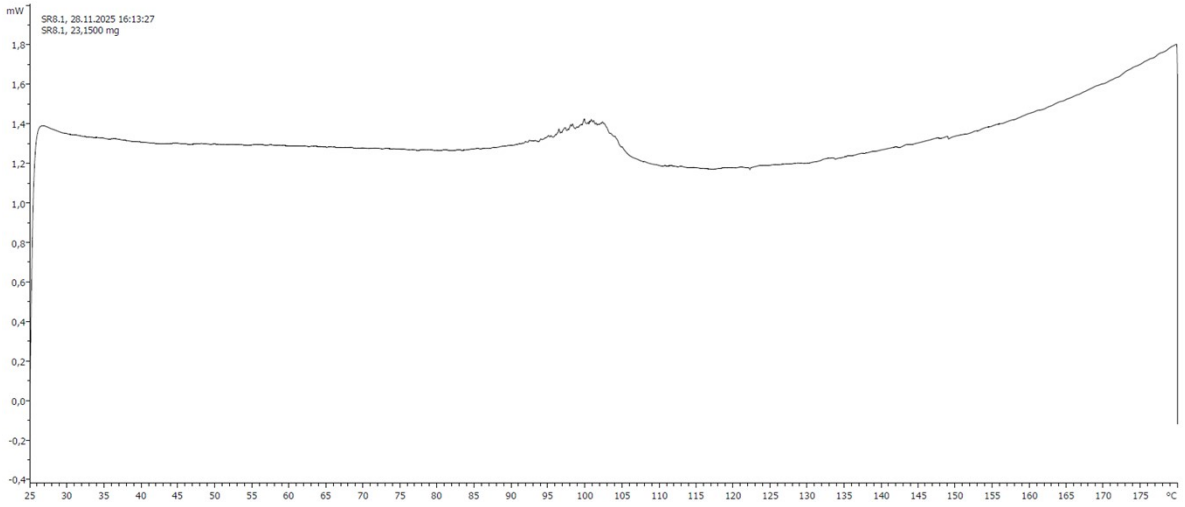

Fig. S20: DSC trace of D2EHPA (30 wt% in Exxsol D120), 50% loaded with Mg(II) up to 180 °C. Heat flow is defined such that a positive flow corresponds to an endothermic event.

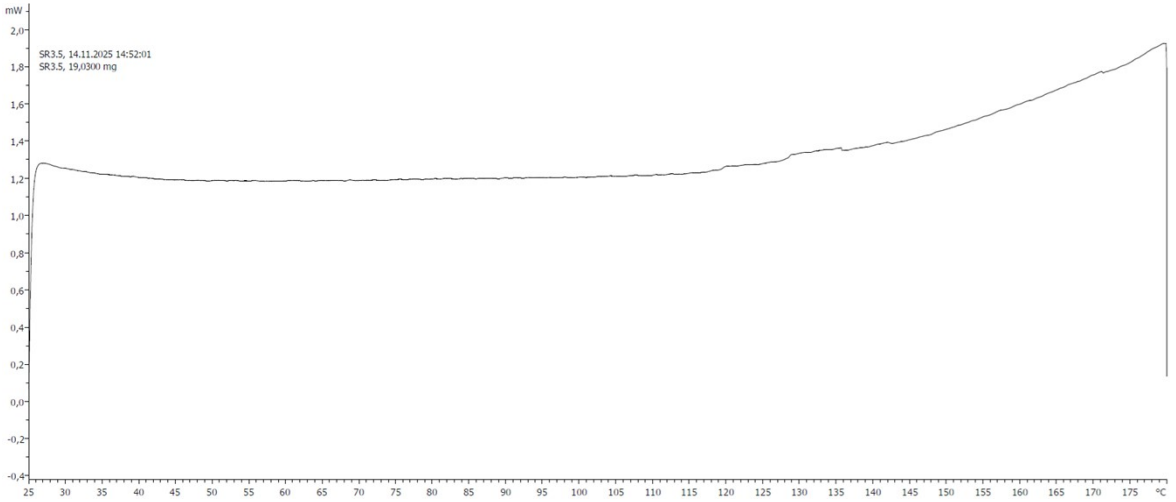

Fig. S21: DSC trace of D2EHPA (30 wt% in Exxsol D120), 50% loaded with Ca(II) up to 180 °C. Heat flow is defined such that a positive flow corresponds to an endothermic event.

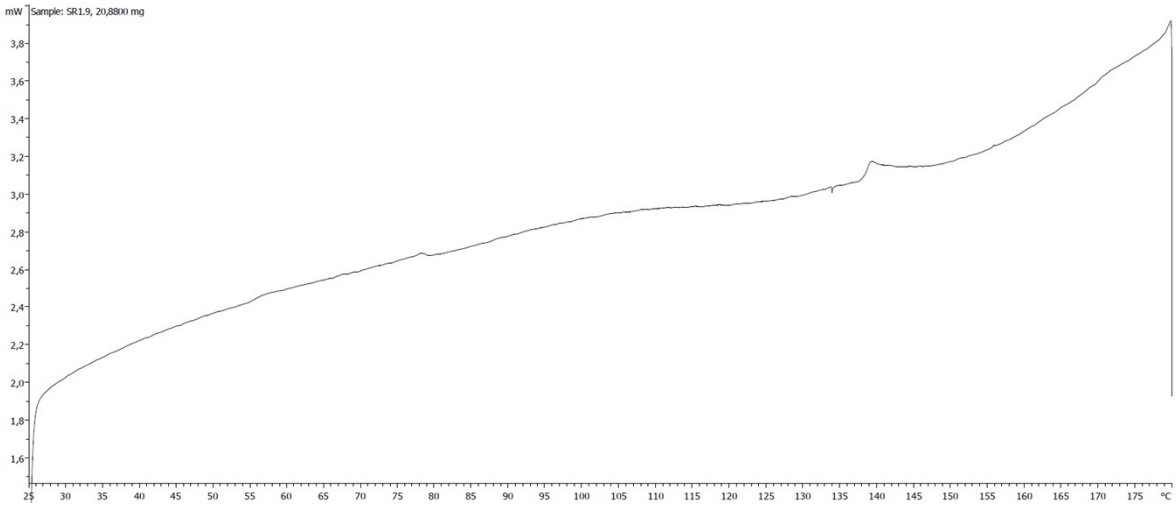

Fig. S22: DSC trace of D2EHPA (30 wt% in Exxsol D120), 100% loaded with Ca(II) up to 180 °C. Heat flow is defined such that a positive flow corresponds to an endothermic event.

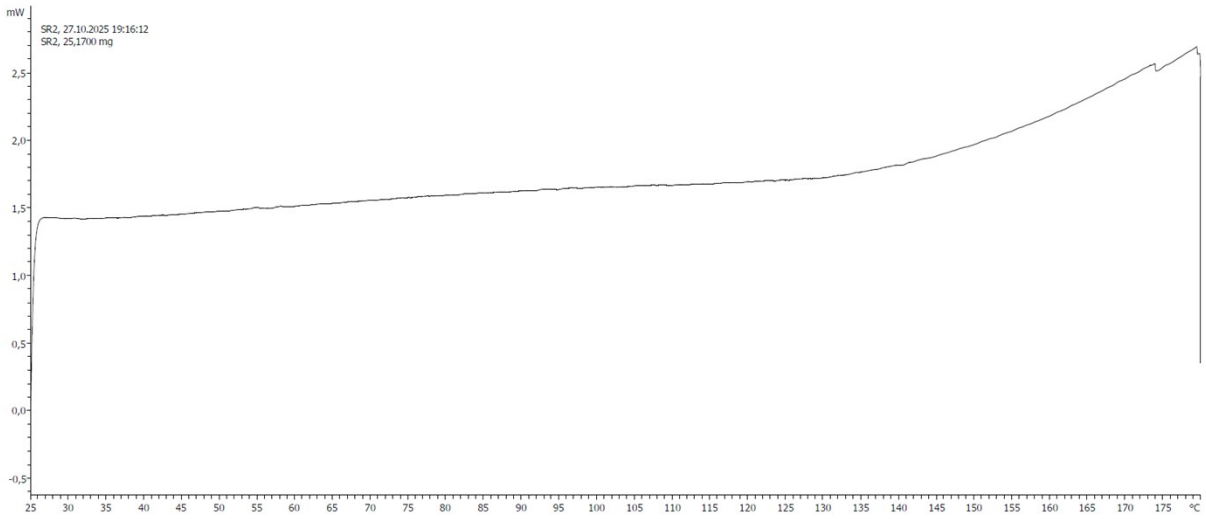

Fig. S23: DSC trace of Ionquest 290 (30 wt% in Exxsol D120), 50% loaded with Ca(II) up to 180 °C. Heat flow is defined such that a positive flow corresponds to an endothermic event.

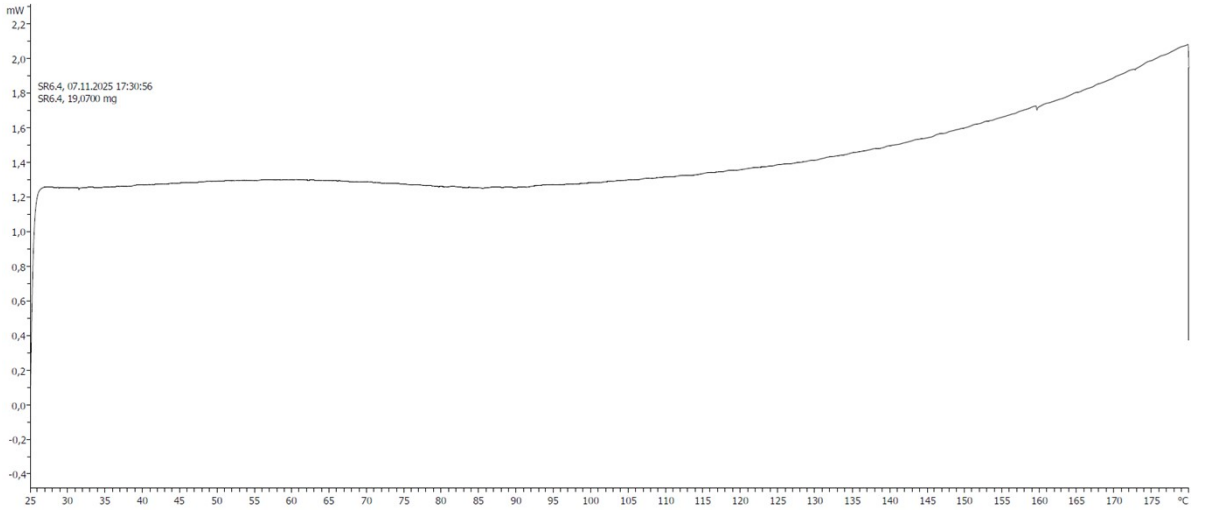

Fig. S24: DSC trace of D2EHPA (30 wt% in Exxsol D120), 30% loaded with Mn(II) up to 180 °C. Heat flow is defined such that a positive flow corresponds to an endothermic event.

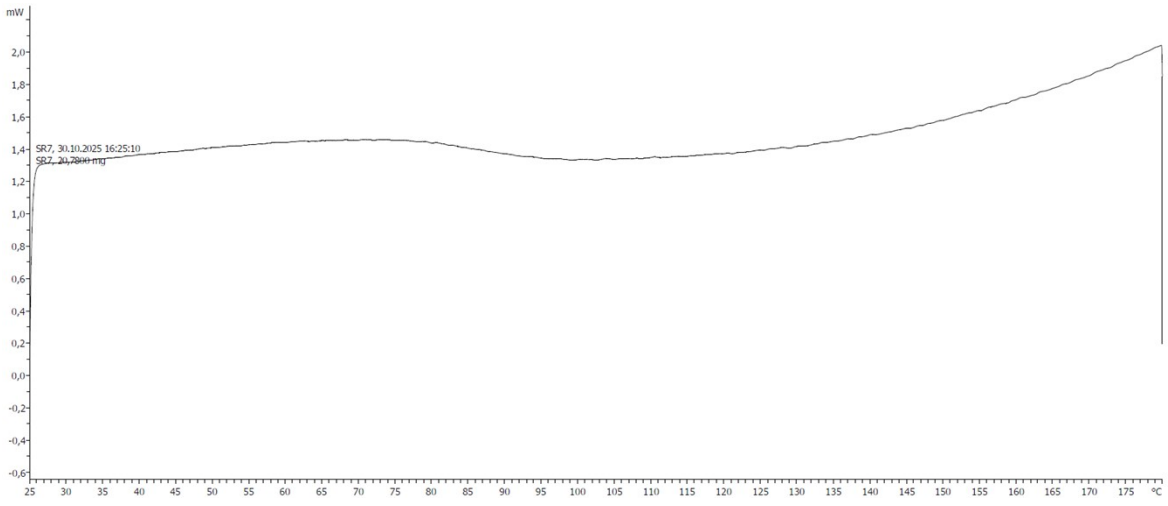

Fig. S25: DSC trace of D2EHPA (30 wt% in Exxsol D120), 50% loaded with Cu(II) up to 180 °C. Heat flow is defined such that a positive flow corresponds to an endothermic event.

^{31}P NMR spectroscopy

The recorded spectra differ vastly in the linewidth of the observed signals. Significant chemical shift differences are also observed, at some degrees of hydration, but their interpretation is not straightforward. A number of factors may influence the linewidth of the observed systems:

- Molecular weight: polymeric structures exhibit rapid spin-spin relaxation (T2) due to slow molecular rotations, which leads to very broad signals
- Sample viscosity: similarly, viscous samples may have shorter spin-spin (T2) and spin-lattice (T2) relaxation times due to slow molecular rotations
- Paramagnetism: the presence of the Ni(II) paramagnetic center may lead to rapid spin-lattice relaxation (T1), broadening signals
- Chemical equilibria: rapid exchange between two chemical environments may lead to line broadening, in an intermediate regime between defined signals at slow exchange and coalescence into an average signal at very rapid exchange

Only a small fraction of the nuclei in the samples (approx. 1% of Ni) are quadrupolar, ruling out quadrupolar relaxation as a significant factor.

Ni(II)–D2EHPA system

^{31}P-NMR spectra for this system are shown in Fig. S23. At the lowest studied degree of hydration, (0.5 eq. of water) the spectrum features a very sharp absorption line, in addition to a broad signal which is visible as a raised baseline. The two signals may correspond to a mononuclear tetrahedral species on one hand, and a polymeric or oligomeric species on the other. The very sharp nature of the band corresponding to the tetrahedral species can be rationalized by invoking the influence of ligand field stabilization energy (LFSE) on the ionic radius off the central metal cation of a coordination complex (see ref. 7, main text). The Ni(II) ion is characterized by a large difference in LFSE between octahedral and tetrahedral coordination, and consequently a significantly larger ionic radius in tetrahedral complexes. The larger bond distances imply weaker coupling between the Ni(II) paramagnetic center and the ligand nuclei, reducing their relaxation rate in tetrahedral complexes with respect to octahedral complexes.

At 2.5 eq. of water, a complex signal is observed consisting of many components. Only two isomers of the complex $NiA_2(H_2O)_2$ exist (*cis* and *trans*), suggesting that oligomeric species occur as well. Broadening may thus in part be due to chemical equilibria. None of the consistent signals is as sharp as that observed at 0.5 eq. of water, however, suggesting that all species are octahedral in nature. Moreover, the large LFSE of octahedral Ni(II) complexes is expected to preclude equilibria with tetrahedral species from occurring.

At higher degrees of hydration, signals are very broad. The degree of broadening greatly exceeds that observed at 2.5 eq. of water, indicating that it cannot only be attributed to rapid ligand exchange equilibria between discrete complexes. The broadening of the signal is accompanied by a visually more rapid decay of the free induction decay (FID) in the time domain, which suggests more rapid relaxation due to reduced mobility of the phosphorus nuclei. This can be interpreted as evidence of the formation of supramolecular structures, which

thus only occurs when more water is present then can be occupied in the inner sphere without the displacement of D2EHPA ligands. Second sphere water does not appear to affect the chemical shift of the signal, suggesting that the species present at saturation with water is identical to that at 6.5 eq. of water, but distinct from that at 2.5 eq. and 4.4 eq.

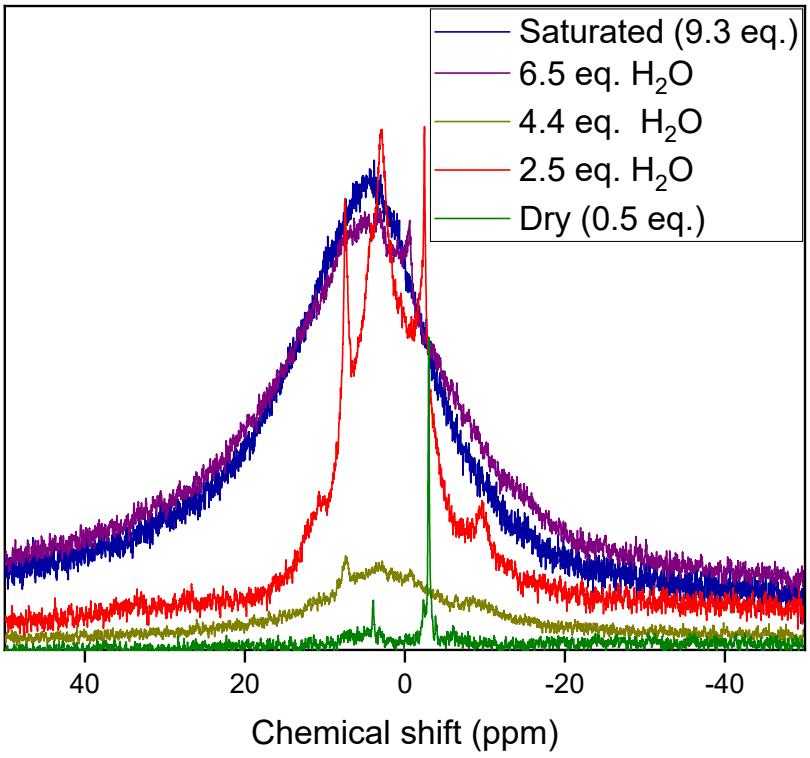

Fig. S26: ^{31}P-NMR spectra of the Ni(II)–D2EHPA system (10 wt% NiA_2 in heptane) at various degrees of hydration (243 MHz).

Ni(II)–Ionquest 290 system

^{31}P-NMR spectra for this system are shown in Fig. S24. The anhydrous sample (0.07 eq. of water) does not display a sharp peak in the signal in the manner that was observed for the least hydrated Ni(II)–D2EHPA sample. Instead, only a very broad, elevated baseline is observed, consistent with the occurrence of coordination polymers, which feature very rapid T2 relaxation rates. This relaxation rate is further enhanced by the high viscosity of the sample.

In accordance with the behavior of the Ni(II)–D2EHPA system, a compound signal is observed at 2.3 eq. of water, consisting of several superimposed peaks. A satisfactory fit was obtained using a 5-peak Lorentzian regression (Fig. S25). Again, as only two isomers exist with stoichiometry $NiA_2(H_2O)_2$, oligomeric complexes must be invoked to clarify the nature of the compound signal. Dimers are expected to give rise to at least two signals, namely bridging and terminal phosphinate ligands, while trimers may result in the emergence of a third peak.

Once again, a single, broad peak is observed at higher hydration numbers, concurrently with an enhanced relaxation rate of the FID and an upfield shift of the signal. Supramolecular structures thus appear to form when the coordination of water requires displacement of extractant molecules from the inner sphere.

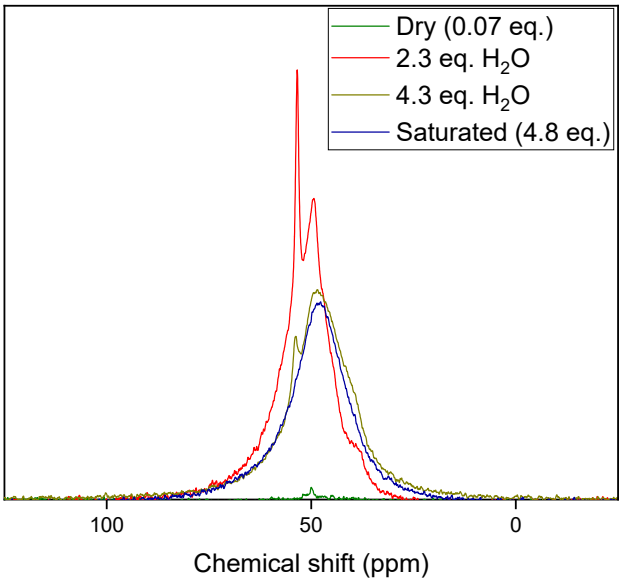

Fig. S27: ^{31}P-NMR spectra of the Ni(II)–Ionquest 290 system (10 wt% NiA_2 in heptane) at various degrees of hydration (243 MHz).

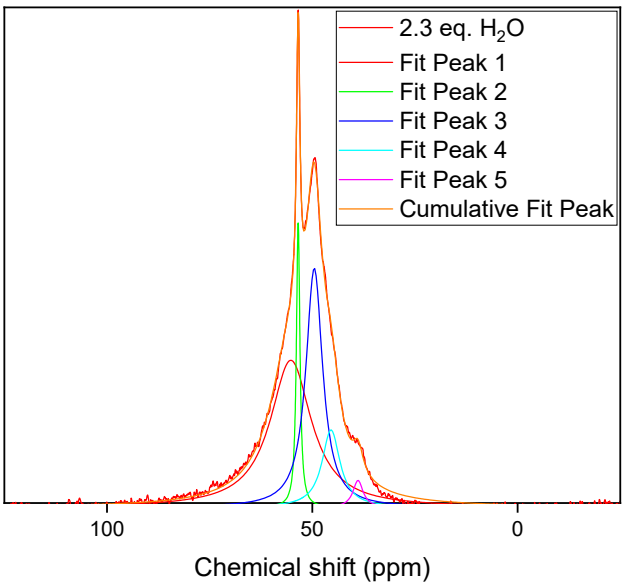

Fig. S28: Deconvolution of the ^{31}P-NMR spectrum of the Ni(II)–Ionquest 290 (10 wt% NiA_2) wit 2.3 eq. of added water (243 MHz). A 5-peak Lorentzian regression was applied.

Supporting photographs

Fig. S29: Ni(II)–Ionquest 290 complex in heptane at various stages of hydration: fully anhydrous (left, in capillary), after contact with air (second from left, in vial), 0.4 eq. Of water (middle, in vial), 2.3 eq.of water (second from right, in vial) and saturated with water (right, in vial).

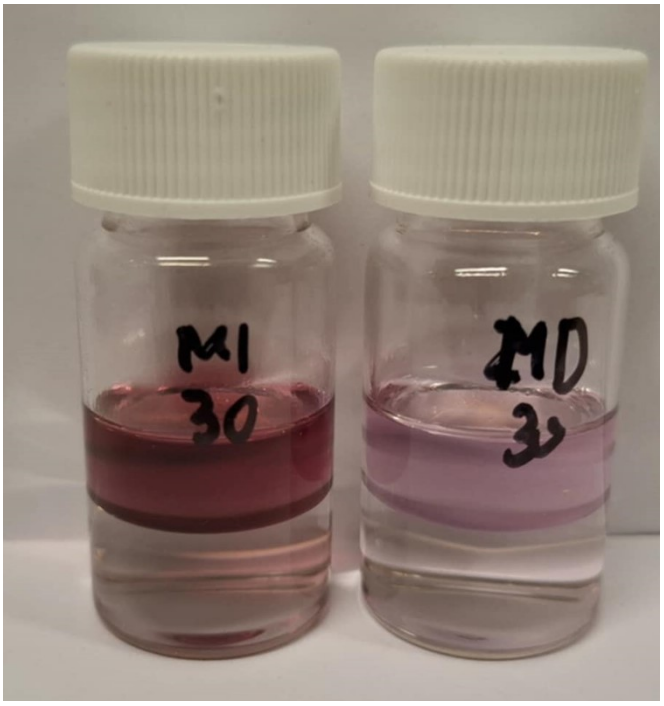

Fig. S30: Mn(II)–Ionquest 290 complex (left, 95 mmol L^{-1}) vs. Mn(II)-D2EHPA complex (right, 114 mmol L^{-1}) in heptane at 30% loading, demonstrating a clear difference in absorptivity.

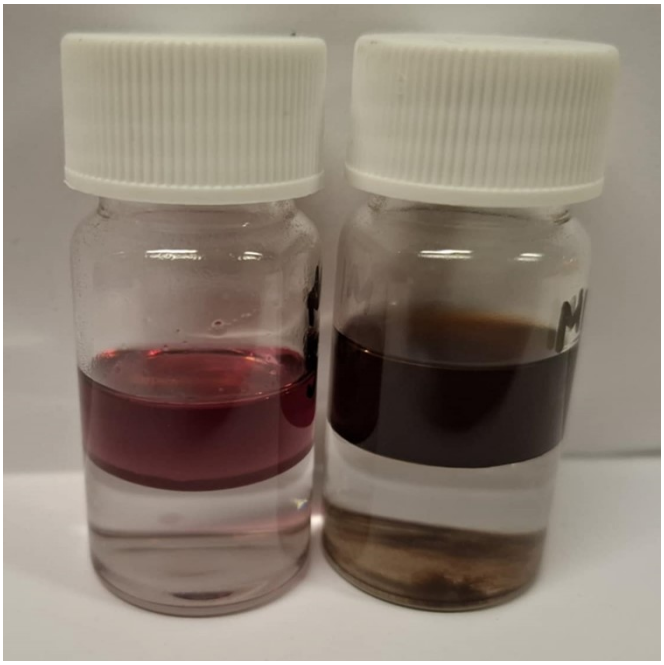

Fig. S31: Mn(II)–Ionquest 290 complex in heptane at 50% loading (left, 158 mmol L^{-1}) vs. 100% loading (right, 315 mmol L^{-1}) in heptane, demonstrating a clear difference in visible hue.